

Membrane amplitude and triaxial stress in twisted bilayer graphene deciphered using first-principles directed elasticity theory and scanning tunneling microscopy

M. Neek-Amal¹, P. Xu², D. Qi², P. M. Thibado², L. O. Nyakiti³, V. D. Wheeler⁴,
R. L. Myers-Ward⁴, C. R. Eddy, Jr.⁴, D. K. Gaskill⁴, and F.M. Peeters¹

¹*Department of Physics, University of Antwerpen,
Groenenborgerlaan 171, B-2020 Antwerpen, Belgium*

²*Department of Physics, University of Arkansas, USA*

³*U.S. Naval Research Laboratory, Washington, District of Columbia 20375, USA*

⁴*Departments of Marine Engineering, Material Science and Engineering,
Texas A&M University, College Station TX, 77843 USA*

(Dated: July 7, 2014)

Twisted graphene layers produce a moiré pattern (MP) structure with a predetermined wavelength for given twist angle. However, predicting the membrane corrugation amplitude for any angle other than pure AB-stacked or AA-stacked graphene is impossible using first-principles density functional theory (DFT) due to the large supercell. Here, within elasticity theory we define the MP structure as the minimum energy configuration, thereby leaving the height amplitude as the only unknown parameter. The latter is determined from DFT calculations for AB and AA stacked bilayer graphene in order to eliminate all fitting parameters. Excellent agreement with scanning tunneling microscopy (STM) results across multiple substrates is reported as function of twist angle.

I. INTRODUCTION

The electronic properties of twisted stacked graphene layers have been the focus of numerous studies [1]. The periodic potential of the interacting substrate is the source of a new set of Dirac points in the energy spectrum of graphene [2]. Also, the van Hove singularity is found to shift with twist angle [3, 4]. For large angles the graphene layers behave like isolated sheets, while for small angles the new Dirac cones result in two van Hove singularities. [5].

Early experimental studies of multi-layer twisted graphene using scanning tunneling microscopy (STM) found a moiré pattern (MP) structure [4]. Such a MP results in an additional corrugation as compared to the untwisted case. The most prominent examples have come from epitaxial graphene grown on SiC [6–8]. From those experimental data, a simple analytic expression for the wavelength of the superstructure was quickly discovered and provided a clear picture of the mechanism as well as the responsible twist angle. Much more difficult, however, is predicting the corrugation amplitude, and so far a simple analytic expression for this does not exist. Theoretical studies about the height deformation of the twisted bilayer graphene are difficult. This is because the large size (e.g. up to 10 nm in size) MP unit cell makes ab-initio calculations infeasible. Only in certain limiting cases the size of the unit cell is sufficiently small that ab-initio calculations are possible [9]. When DFT results can be obtained they set the standard for all other approaches. Consequently, it is best to parameterize any new approach such that it agrees with the DFT results in certain limits [11–13]. Nevertheless, there exist alternative methods that show promise using classical interatomic potentials [14].

Here we present an analytical approach for the height deformation of twisted bilayer graphene without using

any fitting parameters and assuming only that the experimentally observed MP structure is the minimum energy configuration. We show that the deformation of the top graphene layer, due to the van der Waals interaction, is affected by the MP pattern. These deformations result in strain which subsequently leads to three-fold symmetry in the curvature and an induced pseudo-magnetic field. We also report excellent agreement with scanning tunneling microscope measurements that we acquired from various multi-layer graphene samples.

II. THE SAMPLES AND STM EXPERIMENTS

Multiple epitaxial graphene samples grown on various miscut (i.e., non-polar m-plane and a-plane surfaces) n+6H-SiC substrates (measuring 16 mm × 16 mm, Ay-mont Technology) were used for this study. Growth was carried out in a commercially available hot-wall Aixtron VP508 chemical vapor deposition reactor. Prior to graphene growth, both SiC substrates were etched in situ in a 100 mbar H₂ ambient at either 1520°C or 1560°C for 50 min. After etching, the ambient condition was switched to Ar, followed by a temperature ramp to 1620°C. The graphene synthesis process was then conducted for 15 minutes up to 60 minutes under a flowing Ar environment of 20 standard liters per min. at 100 mbar, with a substrate temperature still at 1620°C. The post-growth morphology was characterized using atomic force microscopy and the multi-layer graphene coverage was confirmed using Raman spectroscopy. After these characterizations, constant-current filled-state STM images were obtained using an Omicron ultrahigh-vacuum (base pressure is 10⁻¹⁰ mbar), low temperature model STM operated at room temperature. The samples were mounted with silver paint onto a flat tantalum sample plate and transferred through a load-lock into the STM

chamber where it was electrically grounded. STM tips were electrochemically etched from 0.25 mm diameter polycrystalline tungsten wire via a custom double lamella method with an automatic gravity-switch cutoff. After etching, the tips were gently rinsed with distilled water; briefly dipped in a concentrated hydrofluoric acid solution to remove surface oxides, and then transferred into the STM chamber. Additional experimental details are provided elsewhere [15].

III. THE MODEL

A. Minimum energy configuration

For a given twist angle θ between two graphene layers, the top sheet is attracted to the bottom sheet due to van der Waals (vdW) interaction. The zero lattice mismatch between the honeycomb lattice structures of the two graphene layers leads to an infinite moiré wavelength L when the two layers have either AB- or AA-stacking. This is because $L = \frac{\sqrt{3}a_0}{2\sin(\theta/2)}$ where $a_0 = 1.42 \text{ \AA}$ is the carbon-carbon bond length, θ is the disorientation angle with respect to AB-stacking having $\theta = 0$, and AA-stacking corresponds to $\theta = \pi/3$. In general the commensurate rotation where a B' atom from the top layer is directly above the A atom in the bottom layer, is moved by the rotation to a position formerly occupied by an atom of the same kind, can be obtained from

$$\theta_n = \cos^{-1}\left[\frac{3n^2 + 3n + 1/2}{3n^2 + 3n + 1}\right], \quad n = 0, 1, 2, \dots \quad (1)$$

For twist angle θ defined with respect to the x -axis (taken along the zigzag chain direction of graphene), we define the out-of-plane deformation of the lattice as $h(\vec{r}, \theta)$ where $\vec{r} = (x, y)$. From experiment we know that the minimum energy configuration for $h(\vec{r}, \theta)$ is the MP structure and depending on the preparation method different twist angles are possible. Furthermore, from continuum elasticity theory the deformation of the membrane over a flat substrate is given by the solution of the following differential equation [16]:

$$(k\nabla^4 - \tau\nabla^2 + v(\vec{r}, \theta))Z(\vec{r}, \theta) = 0, \quad (2)$$

where $Z(\vec{r}, \theta)$ is the height of the membrane at \vec{r} , k and τ correspond to the bending and stretching modulus of graphene and $v(\vec{r}, \theta)$ depends on the vdW parameters between the two layers and is proportional to the Hamker constant. The Fourier transform (FT) of the solution of Eq. (2) must have six moiré pattern vectors [2, 17–19], i.e., $\vec{G}_m = \mathcal{R}_{\phi_m}\vec{G}_0$ with $m = 0, 1, \dots, 5$ where $\vec{G}_0 = (1 - \mathcal{R}_\theta)(0, 2\kappa)$ with $\kappa = \frac{2\pi}{3a_0}$ and \mathcal{R}_{ϕ_m} (and \mathcal{R}_θ) is the rotation matrix about the z -axis over an angle $\phi_m = \frac{2\pi m}{6}$ (and θ).

Therefore, for $\theta > 0$ the height deformation of graphene can be written as

$$h(\vec{r}, \theta) = h_0(\theta)f(\vec{r}, \theta) \quad (3)$$

where the modulation function is $f(\vec{r}, \theta) = \sum_m e^{i\vec{G}_m \cdot \vec{r}}$ [19], and $h_0(\theta)$ should be determined using microscopic information (the zero reference height is taken to be the AB-stacking interlayer position, i.e. $Z(\vec{r}, \theta) = d_{AB} + h(\vec{r}, \theta)$, and corresponds to the minimum energy configuration). For a given twist angle we can simplify the modulation function as

$$h = 2h_0(\theta)\left\{\cos[\vec{r} \cdot \vec{G}_0] + 2\cos\left[\frac{\vec{r} \cdot \vec{G}_0}{2}\right]\cos\left[\frac{\sqrt{3}}{2}|\vec{r} \times \vec{G}_0|\right]\right\}. \quad (4)$$

In order to better visualize and to compare it with experimental data, we plot this function in Fig. 1 for two typical twist angles of 1.59° in (a) and 1.88° in (d). A plethora of STM images showing various MP (not all shown) from various substrates were collected together in order to experimentally test the theory. The two items we accurately measure from the STM images are the average wavelength as well as the average amplitude of the MPs. From the wavelength measurement we convert to twist angle using the formula mentioned earlier. For the amplitude measurements, two situations arise. When the amplitude of the MP is large, similar to the STM images shown in Figs. 1(b,e), it is easy to determine the amplitude from the height cross section plots similar to the ones shown in Figs. 1(c,f). Here, we show two height cross sections from Figs. 1(a,d) along the solid black lines and compare them with our experimental results (symbols) from Figs. 1(b,e).

Notice that the height profile obtained from STM measurements give us the total height which contains contributions from both electronic and atomic corrugations [10]. The presented theory in this work addresses only the atomic corrugations. The electronic contributions depends on the used bias voltage and the STM measurements conditions. In Ref. [3], a maximum of 50% of the total height was found to be due to the atomic corrugations. However, when the amplitude is small the STM image shows a superposition of the MP structure and the one due to the atomic electronic corrugation. The electronic corrugation due to the individual atoms is not part of the theory. For these STM images, we measure the membrane amplitude by measuring the height change from the top of the electronic corrugation at the top of the MP to the top of the electronic corrugation at the bottom of the MP. For flat graphene or graphite this height change gives zero. Note it is possible that the electronic corrugation of the carbon atoms at the top of the MP is slightly different when compared to the bottom of the MP; however we expect this to be minute given the large wavelengths and small amplitudes. The full collection of experimental STM results for membrane height versus twist angle is shown in Fig. 2 as symbols. Notice the excellent agreement between theory and experiment, which supports the idea that any electronic variation is small.

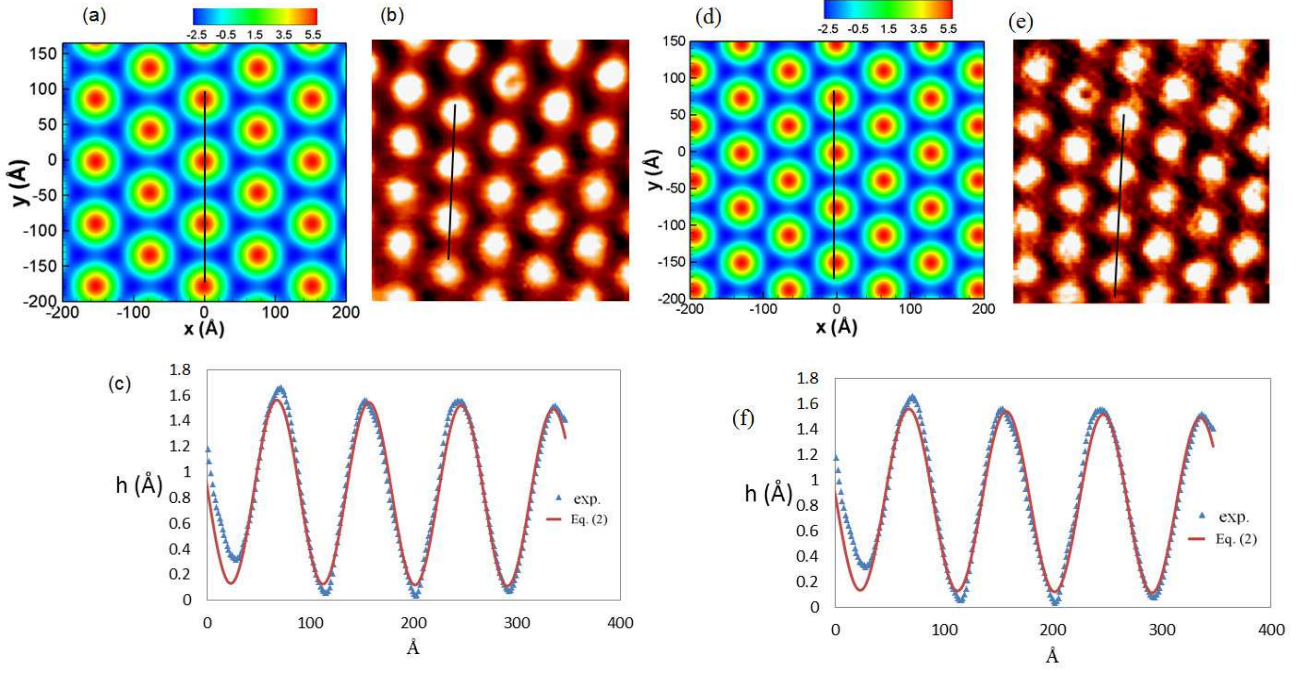


FIG. 1: Height deformation of a graphene sheet over graphene: (a,d) are the results from Eq. (4) and corresponding filled-state (0.05 V), constant-current (1.0 nA) STM images (b,e) for twist angles $\theta = 1.59^\circ$ (a,b,c) and $\theta = 1.88^\circ$ (d,e,f). In (c,f) we show two cross sections along indicated solid black lines in the top figures.

IV. ENERGETIC CONSIDERATION AND STRAIN TENSOR

In order to have a real predictive theory we still need to calculate $h_0(\theta)$. In order to do so, we first write the elastic energy as given by

$$E_{el} = \frac{1}{2} \int [k(\nabla^2 h)^2 + \lambda \varepsilon_{\ell\ell}^2 + 2\mu \varepsilon_{ij}^2] d\vec{r}, \quad (5)$$

where $k \simeq 1.1 \text{ eV}$ is the bending rigidity of graphene and $\lambda = 3.5 \text{ eV \AA}^{-2}$ and $\mu = 8 \text{ eV \AA}^{-2}$ are the Lamé coefficients. The elements of the strain tensor can be found using $\epsilon_{\alpha\beta} = \frac{1}{2}(\partial_\beta u_\alpha + \partial_\alpha u_\beta) + \frac{1}{2}\partial_\alpha h \partial_\beta h$:

$$\begin{aligned} \varepsilon_{xx} &= 4h_0^2(\vec{G}_0 \cdot \vec{\chi})^2, \varepsilon_{yy} = 4h_0^2|\vec{G}_0 \times \vec{\chi}|^2, \\ \varepsilon_{xy} &= 4h_0^2(\vec{G}_0 \cdot \vec{\chi})|\vec{G}_0 \times \vec{\chi}| \\ \vec{\chi} &= \left\{ \sin\left[\frac{\vec{r} \cdot \vec{G}_0}{2}\right] \left(2 \cos\left[\frac{\vec{r} \cdot \vec{G}_0}{2}\right] + \cos\left[\frac{\sqrt{3}}{2}|\vec{r} \times \vec{G}_0|\right] \right), \sqrt{3} \sin\left[\frac{\sqrt{3}}{2}|\vec{r} \times \vec{G}_0|\right] \cos\left[\frac{\vec{r} \cdot \vec{G}_0}{2}\right] \right\}. \end{aligned}$$

For the in-plane components (first term in parenthesis) we assume that the top layer is in its minimum energy configuration (MP structure) and the coordinate (\vec{r}) in our analysis is written in the deformed system, thus we do not add them to the out-of-plane components of the strain tensor (see appendix). Diagonalising the strain

tensor gives the principal axis with eigenvalues

$$\epsilon_{\pm} = \frac{1}{2}[\epsilon_{ll} \pm |\vec{A}|], \quad (6)$$

where \vec{A} is the gauge vector corresponding to the lattice deformation [21]. Surprisingly, we found that $\epsilon_- = 0$ (since $\epsilon_{xx}\epsilon_{yy} = \epsilon_{xy}^2$) and that $\epsilon_+ = |\vec{A}|$ has MP symmetry.

Since the eigenvalue $\epsilon_- = 0$, we conclude that the stress along the corresponding eigenvector results in no lattice deformation. These principle directions correspond to the most tensile and compression directions in graphene, i.e.

$$\Phi_+ = \frac{1}{2} \tan^{-1}\left(\frac{-A_y}{A_x}\right), \quad \Phi_- = \frac{1}{2} \tan^{-1}\left(\frac{A_x}{A_y}\right). \quad (7)$$

Solution of the integrals in Eq. (5) for a given θ can be simplified to

$$E_{el} = h_0^2(\theta)[g_b(\theta) + h_0^2(\theta)g_s(\theta)], \quad (8)$$

where we found $g_i(\theta)$ by numerical integration (a_i, b_i are also fitting parameters) over the corresponding MP unit cell which has the following polynomial dependence:

$$g_{b,s}(\theta) \cong (a_{b,s} + b_{b,s}\theta^2)^2. \quad (9)$$

In our recent work [18], we presented an atomistic simulation showing that the local vdW energy stored between two layers also exhibits a moiré pattern structure. Here using the latter idea we write the binding energy as

$$E_{bin} = E_{AB} - \delta E \left(1 - \frac{\eta(\theta)}{\eta(0)}\right), \quad (10)$$

where $E_{AB} \sim 50\text{-}60\text{ meV/atom}$ is the binding energy between two graphene layers in AB-stacking and $\delta E = E_{AB} - E_{AA} (\approx 13 - 15\text{ meV/atom})$ as found from DFT in Ref. [13]. **The binding energy varies with interlayer distance as d^{-4} , but here we only model its variation with θ and the in-plane coordinates because we are only interested in the change in height, and not in its absolute position.** Notice how this parameterization incorporates the known DFT results. Note that the bright feature in all moiré patterns is where we have local AA stacking of graphene. We can understand this by realizing that in between two adjacent AA stacks there is a low energy AB (i.e., Bernal) stacked region. Since carbon atoms in an AA stack have higher energy as compared to the one for the AB stack we expect larger amplitude in the AA stacked region, i.e. the AB stacked planes are closer together as compared to the AA stacked planes.

We introduce the function $\eta(\theta)$ in Eq. (10) based on the MP as

$$\eta(\theta) = \int f(\vec{r}, \theta) d\vec{r}, \quad (11)$$

which expresses the spacial average of the modulation function over graphene.

V. HEIGHT PROFILE AND PSEUDO-MAGNETIC FIELD

In mechanical equilibrium, the binding energy is competing with the bending energy (elastic energy), and we must have

$$E_{el} = E_{bin}. \quad (12)$$

Solution of the latter equation results in the following dependence for $h_0(\theta)$

$$h_0^2(\theta) = -\frac{g}{2} + \left[\frac{g^2}{4} + \frac{4}{3a_0^2} \frac{(E_{AB} - \delta E(1 - \frac{\eta(\theta)}{\eta(0)}))}{g_s} \right]^{1/2}, \quad (13)$$

where $g = g_b/g_s$. Because $g_b/g_s \ll 1$ we can approximate h_0 as

$$h_0 \cong \left[\frac{4}{3a_0^2} \frac{(E_{AB} - \delta E(1 - \frac{\eta(\theta)}{\eta(0)}))}{(a_s + b_s\theta^2)^4} \right]^{1/4} \sim \theta^{-1}, \quad (14)$$

for $\theta > 1^\circ$. Notice that the difference between the maximum and the minimum of h in Eq. (4) is given by $\Delta h = 8h_0$. $(E_{bin} - E_{AB})/(-\delta E)$ approaches 1 when $\theta \rightarrow \pi/3$. Our prediction resulting from Eq. (13) for the overall height of the membrane (i.e. $8h_0$) is shown versus twist angle in Fig. 2 and compared with our experimental results.

We collected a variety of STM images of various multi-layer graphene moiré patterns (not all are shown) from a-plane and m-plane SiC substrates grown under similar conditions. Five typical line profiles extracted from these STM images and having varying wavelength and amplitude are shown in Fig. 2(a). The line profiles are ordered from top to bottom based on decreasing amplitude. Notice the lowest line profile has, superimposed on it, an even smaller amplitude and higher frequency signal. This is the electronic corrugation of the carbon atoms, and it is worth pointing out how small the electronic amplitude is when compared to the membrane corrugation. The membrane corrugation persists when imaging the moiré pattern through a range of normal bias voltage settings (± 0.05 to ± 1.00 V) and tunneling current setpoints (0.05 to 1.00 nA). For example, when a moiré pattern with a wavelength of 4 nm is repeatedly imaged while incrementally altering the bias voltage from ± 0.01 V to ± 1.0 V with a tunneling current setpoint of 0.5 nA we see only a small amplitude variation as shown in a semi-log plot of Fig. 2(b). Within the error bars, the membrane amplitude is relatively unchanged.

A plot showing the membrane amplitude as a function of twist angle is shown in Fig. 2(c). Even though it is possible that the electronic amplitude is slightly different at the crest of the membrane compared to the trough of the membrane, we believe this is within the error bars of our results. Also, unlike the image contrast inversion STM data acquired from single crystal metal surfaces [10], for twisted graphene on graphene/SiC we do not see any significant height changes in the moiré pattern as we vary the STM tunneling condition.

It is also worthwhile to mention that the low energy electronics of the deformed graphene can be obtained from the modified Dirac equation due to the modified hopping parameters from the tight-binding model which are now a function of the atomic positions $t(\mathbf{r})$ [20]. The Dirac Hamiltonian in the effective mass approximation

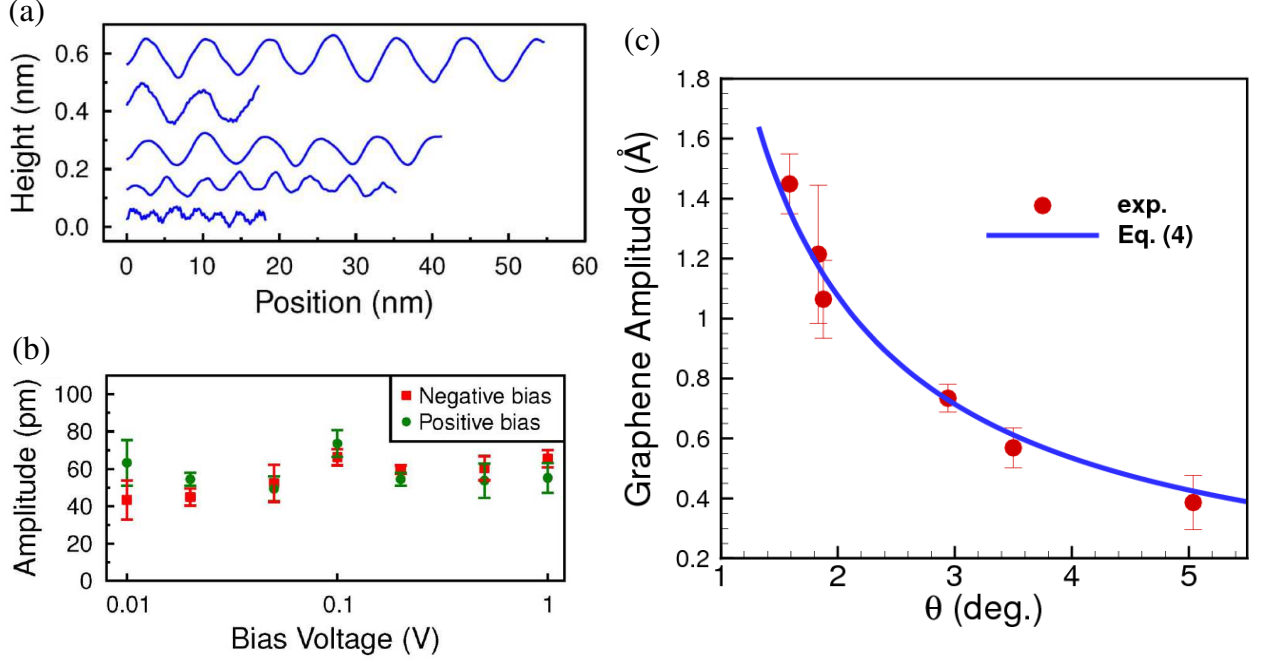


FIG. 2: (a) Five typical constant-current height line profiles extracted from STM images acquired with a variety of tunneling setpoint conditions. (b) Constant current (0.5 nA) STM image derived data showing the average membrane amplitude versus bias voltage setpoint using a semi-log plot for twist angle 3.5° . (c) STM image derived data (symbols) showing the average membrane amplitude versus twist angle. For the STM data we measure the wavelength ($\sim \pm 0.1$ nm) and convert to twist angle. The solid line is the result of the presented theory, i.e. Eq. (13).

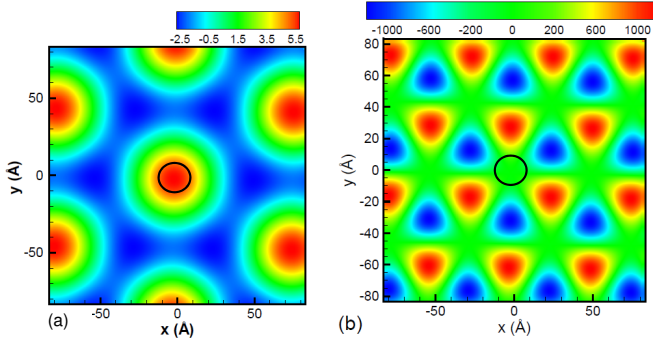


FIG. 3: Height deformation (h/h_0) of graphene over a graphene sheet, i.e. Eq. (4), for twist angle $\theta = 1.59^\circ$ (a) and corresponding pseudo-magnetic field in units of h_0^2 (b), obtained from Eq. (15). The circle in (a), (b) indicate the regions with extreme height and zero magnetic field, respectively.

in the presence of lattice deformation (here out-of-plane deformation) introduces strain which induces an effective gauge field $\vec{A} = \frac{2\beta_0\hbar}{3a_0e}(\varepsilon_{xx} - \varepsilon_{yy}, -2\varepsilon_{xy})$ where β_0 ($\sim 2-3$) is a constant [21]. Using the strain tensor components

we found an analytical expression for B as function of θ .

$$B = \frac{2\beta_0\hbar}{3a_0e}(\varepsilon_{xx,x} - \varepsilon_{yy,x} + 2\varepsilon_{xy,y}). \quad (15)$$

We plot the height deformation (h) in units of h_0 in Fig. 3(a) and the corresponding pseudo-magnetic field in units of h_0^2 for $\theta = 1.59^\circ$ in Fig. 3(b). The pseudo-magnetic field has three-fold symmetry and it is surprising that inside each MP unit cell the field vanishes at the position of the extrema in the height deformation (see the circles in Fig. 3). It is also worthwhile to mention that our study realizes in a natural way the proposal for triaxial stress creation in graphene proposed by F. Guinea *et al.* [22] by using twisted graphene sheets.

VI. SUMMARY

In summary, we presented a theory for the out-of-plane deformation of a twisted graphene sheet due to the vdW interaction with a graphene substrate. By defining the MP structure, for the out-of-plane deformation, as the minimum energy configuration we derive an analytic solution without any fitting parameters. We found excellent agreement for the height variation with our STM data for different twist angles.

Acknowledgment: This work was supported by the Flemish Science Foundation (FWO-VI) and the Methusalem Foundation of the Flemish Government. M.N.-A was supported by the EU-Marie Curie IIF post-doc Fellowship 299855. P.M.T. is thankful for the financial support of the Office of Naval Research under Grant No. N00014-10-1-0181 and the National Science Foundation under Grant No. DMR-0855358. L.O.N. acknowledges the support of the American Society for Engineering Education and Naval Research Laboratory Postdoctoral Fellow Program. Work at the U.S. Naval Research Laboratory is supported by the Office of Naval Research.

VII. APPENDIX

The in-plane displacement vector for micron size graphene flake can be written as

$$\vec{U} = \sum_{m,n} \vec{u}(\vec{r} + \vec{T}_{m,n}(\theta)), \quad (16)$$

where the summation is taken over all MP unit cells and inside each MP unit cell (see circles in Fig. 3) one can write $\vec{u}(\vec{r}, \theta) = C(\theta)(2xy, x^2 - y^2)$ are the in-plane components of the strain tensor, $\vec{T}_{m,n}(\theta)$ is the translation vector of the MP lattice, and C is a twist angle dependent variable which determines the strength of the in-plane strain. The corresponding in-plane strain elements written for each MP unit cell are given by

$$\varepsilon_{xx} = 2Cy, \varepsilon_{yy} = -2Cy, \varepsilon_{xy} = 2Cx \quad (17)$$

and the corresponding pseudo-magnetic field is a function of twist angle but independent of position, i.e. $\frac{16C\beta_0\hbar}{3a_0e}$. The corresponding principal axes are independent of twist angle, i.e. the most tensile and compression directions in graphene are $\frac{1}{2}\tan^{-1}(\frac{-x}{y})$ and $\frac{1}{2}\tan^{-1}(\frac{y}{x})$, respectively, e.g. along $y = x$ line two angles are $\pm\pi/8$.

-
- [1] J. M. B. Lopes dos Santos, N. M. R. Peres, and A. H. Castro Neto, Phys. Rev. Lett **99**, 256802 (2007); Wen-Yu He, Zhao-Dong Chu, and Lin He, Phys. Rev. Lett **111**, 066803 (2013); E. Suárez Morell, M. Pacheco, L. Chico, and L. Brey, Phys. Rev. B **87**, 125414 (2013)
 - [2] K. Watanabe, T. Taniguchi, P. Jarillo-Herrero, P. Jacquod, and B. J. LeRoy, Nature Phys. **8**, 382 (2012).
 - [3] I. Brihuega, P. Mallet, H. Gonzalez-Herrero, G. Trambly de Laissardiere, M. M. Ugeda, L. Magaud, J. M. Gomez-Rodriguez, F. Yndurin, and J.-Y. Veuillen, Phys. Rev. Lett. **109**, 196802 (2012).
 - [4] Eva Y Andrei, G. Li, and X. Du, Rep. Prog. Phys. **75**, 056501 (2012).
 - [5] Zhao-Dong Chu, Wen-Yu He, and Lin He Phys. Rev. B **87**, 155419 (2013); Wei Yan, Mengxi Liu, Rui-Fen Dou, Lan Meng, Lei Feng, Zhao-Dong Chu, Yanfeng Zhang, Zhongfan Liu, Jia-Cai Nie, and Lin He Phys. Rev. Lett. **109**, 126801 (2012); Taisuke Ohta, Jeremy T. Robinson, Peter J. Feibelman, Aaron Bostwick, Eli Rotenberg, and Thomas E. Beechem Phys. Rev.
 - [6] J. Hass, F. Varchon, J. E. Milln-Otoya, M. Sprinkle, N. Sharma, W. A. de Heer, C. Berger, P. N. First, L. Magaud, and E. H. Conrad, Phys. Rev. Lett. **100**, 125504 (2008).
 - [7] X. Li, W. Cai, Jinho An, S. Kim, J. Nah, D. Yang, R. Piner, A. Velamakanni, I. Jung, E. Tutuc, S. K. Banerjee, L. Colombo, R. S. Ruoff, Science **324**, 1312 (2009).
 - [8] M. Ostler, I. Deretzi, S. Mammadov, F. Giannazzo, G. Nicotra, C. Spinella, Th. Seyller, and A. La Magna, Phys. Rev. B **88**, 085408 (2013).
 - [9] G. Giovannetti, P. A. Khomyakov, G. Brocks, P. J. Kelly, and J. van den Brink, Phys. Rev. B **76**, 073103 (2007).
 - [10] S. Heinze, S. Blgel, R. Pascal, M. Bode, and R. Wiesendanger, Phys. Rev. B **58**, 16432 (1998).
 - [11] L. Spanu, Sandro Sorella, and Giulia Galli, Phys. Rev. Lett **103**, 196401 (2009).
 - [12] A. K. Geim and I. V. Grigorieva, Nature (London) **499**, 419 (2013).
 - [13] X. Chen, F. Tian, C. Persson, W Duan, and N-xian Chen, Scientific Reports **3**, 3406 (2013).
 - [14] Irina V. Lebedeva, Andrey A. Knizhnik, Andrey M. Popov, Yurii E. Lozovikda and Boris V. Potapkin, Phys. Chem. Chem. Phys. **13**, 5687, (2011).
 - [15] P. Xu, M. L. Ackerman, S. D. Barber, J. K. Schoelz, P. M. Thibado, V. D. Wheeler, L. O. Nyakiti, R. L. Myers-Ward, C. R. Eddy, Jr., and D. K. Gaskill, Surface Science **617**, 113 (2013).
 - [16] M. Neek-Amal and F. M. Peeters, Phys. Rev. B **85**, 195445 (2012).
 - [17] S. Tang, H. Wang, Y. Zhang, A. Li, H. Xie, X. Liu, L. Liu, T. Li, F. Huang, X. Xie, and M. Jiang, Scientific Reports **3**, 2666 (2013).
 - [18] M. Neek-Amal and F. M. Peeters, Appl. Phys. Lett. **104**, 041909 (2014).
 - [19] J. R. Wallbank, A. A. Patel, M. Mucha-Kruczynski, A. K. Geim, and V. I. Fal'ko, Phys. Rev. B **87**, 245 (2013).
 - [20] M. Neek-Amal, L. Covaci, Kh. Shakouri, and F. M. Peeters, Phys. Rev. B **88**, 115428 (2013); M. Neek-Amal, L. Covaci, and F. M. Peeters, Phys. Rev. B **86**, 041405 (2012); M. Neek-Amal and F. M. Peeters Phys. Rev. B **85**, 195446 (2012).
 - [21] A. H. Castro Neto, F. Guinea, N. M. R. Peres, K. S. Novoselov, and A. K. Geim, Rev. Mod. Phys. **81**, 109162 (2009).
 - [22] F. Guinea, M. I. Katsnelson, and A. K. Geim, Nat. Phys. **2**, 31 (2010).